Chemical Science

EDGE ARTICLE

View Article Online
View Journal | View Issue

Cite this: *Chem. Sci.*, 2019, **10**, 7466

All publication charges for this article have been paid for by the Royal Society of Chemistry

Dynamic colloidal nanoparticle assembly triggered by aptamer–receptor interactions on live cell membranes†

Linlin Yang,[a] Lingyan Meng,[c] Jiaying Song,[a] Yue Xiao,[a] Ruowen Wang,[b] Huaizhi Kang*[ab] and Da Han *[b]

Cells use dynamic systems such as enzyme cascades and signaling networks to control cellular functions. Synthetic dynamic systems that can be target-responsive have great potential to be applied for biomedical applications but the operation of such dynamic systems in complex cellular environments remains challenging. Here, we engineered an aptamer and DNA displacement reaction-based dynamic system that can transform its nanostructure in response to the epithelial cell adhesion molecule (EpCAM) on live cell membranes. The dynamic system consisted of a core nanoparticle and small satellite nanoparticles. With the modifications of different DNA hairpin strands and swing arm strands partially hybridized with an aptamer that specifically recognizes the EpCAM, the two separated particles can dynamically assemble into a core–satellite assembly by aptamer–receptor interactions on the cell membrane surface. The structural change of the system from separated particles to a core–satellite assembly generated plasmonic coupled hot spots for surface-enhanced Raman scattering (SERS) for sensitively capturing the dynamic structural change of the nanoassembly in the cellular environment. These concepts provide strategies for engineering dynamic nanotechnology systems for biological and biomedical applications in complex biological environments.

Received 3rd June 2019
Accepted 21st June 2019

DOI: 10.1039/c9sc02693b

rsc.li/chemical-science

Introduction

Life is sustained by complex systems operating with dynamic reactions. Artificial dynamic systems that can be responsive to environmental stimuli and precisely adjust their physicochemical properties will greatly facilitate the development of biological and biomedical applications, such as imaging, diagnosis and disease treatment.[1–4] For instance, a dynamic nanoassembly was reported to be able to alter the surface display of targeting ligands and thus control its cellular uptake properties.[5] Another example is a nanoparticle system that was designed to dynamically shrink from 100 nm to 10 nm to achieve deep penetration into tumor tissue.[6] Similarly, an Au nanoparticle assembly that was pH-sensitive was applied as a smart drug delivery platform with tumor microenvironmental responsive ability for anti-tumor therapy.[7]

In recent years, dynamic DNA nanotechnology has been an appealing tool to engineer precisely controlled dynamic systems, which are based on the remarkable merits of high specificity, predictability and programmability of DNA Watson–Crick base pairing.[8–10] In particular, a series of DNA nanomachines such as DNA robots,[11–13] molecular motors,[14–16] autonomous walkers[17–20] and logical computers[21–23] have been designed and implemented experimentally. The next step should be applying them for more complex biological applications. However, the design and implementation of dynamic DNA-based systems that automatically carry out functions in complex cellular environments present two critical challenges in molecular engineering. The first one is finding an effective driving force that can precisely control dynamic systems in complex biological environments. Compared to other reactions such as enzyme or DNAzyme-mediated hydrolysis reactions which need enzymes or cofactors (metal ions, *etc.*) that are either difficult to deliver or requiring strict conditions to functionalize in cells to provide energies for dynamic systems,[15,24–26] DNA displacement reactions present some unique advantages. For instance, they are completely enzyme-free reactions, which means that these DNA strand displacement-based dynamic systems can be initiated and driven solely by the DNA molecules in cells. In addition, these DNA displacement reactions are well characterized by various physical or chemical methods and can be even simulated by well-designed *in silico* programs. All of

[a]*Pen-Tung Sah Institute of Micro-Nano Science and Technology, Xiamen University, Xiamen, Fujian, 361005, China. E-mail: kang@xmu.edu.cn*

[b]*Institute of Molecular Medicine, Renji Hospital, School of Medicine, Shanghai Jiao Tong University, Shanghai, 200127, China. E-mail: dahan@sjtu.edu.cn*

[c]*College of Chemistry and Chemical Engineering, Xiamen University, Xiamen, Fujian, 361005, China*

† Electronic supplementary information (ESI) available. See DOI: 10.1039/c9sc02693b

these advantages of DNA displacement reactions provide good opportunities for controlling dynamic systems in complex biological environments. The second challenge is employing an effective component that can bridge dynamic DNA-based systems and interactive biomolecules such as proteins in cells without influencing the programmability and versatility. A common regulation paradigm used in previous reports is genetic editing, which requires sophisticated and cell-wide coordination. Aptamers, which are single-stranded oligonucleotides, have the promising properties of recognizing and regulating biological molecules in the cellular environment.[27,28] In addition, since an aptamer is essentially a single-stranded oligonucleotide, it can be seamlessly encoded in dynamic DNA-based systems with an extended scope of functions, from simple DNA base-pairing reactions to more complicated biomolecular reactions such as DNA–protein interactions.[29,30]

Herein, we explored the use of DNA aptamer and DNA displacement reactions as molecular keys to operate the colloidal nanoparticle assembly in the cellular environment. The system consisted of a spatially separated core nanoparticle and small satellite nanoparticles. The assembly of the two types of particles can be controlled in response to the epithelial cell adhesion molecule (EpCAM) that is an overexpressed cell surface receptor of multiple adenocarcinomas cells.[31,32] Compared to the intracellular genomic or transcriptional marker molecules, cell-surface receptors, mostly membrane proteins, are excellent candidates as molecular signatures for cellular applications such as smart control of the dynamic assembly process *in situ* due to their excellent specificity, accessibility and scalability. The conformational changes of the system from separated particles to a core–satellite assembly provided plasmonic coupled hot spots for SERS detection. Owing to its distinct advantages of low background, insensitivity to photobleaching or quenching, single-molecule sensitivity and fingerprint-like spectra,[33–36] we are able to use SERS to monitor the performance of this nanoparticle assembly in the cellular environment. This dynamic nanoparticle system explored the use of aptamers and DNA displacement reactions to assemble the nanostructures in response to cell surface biomarkers. Therefore, it provides strategies for engineering dynamic systems for mediating cellular functions as well as intracellular imaging in complex biological environments.

Results and discussion

The overall concept and proposed strategy of constructing the aptamer-based dynamic colloidal nanoparticle assembly is depicted in Fig. 1. Au nanoparticles (AuNPs) with diameters of 50 and 13 nm (Fig. S1†) were used as the core and satellites to assemble the core–satellite assembly. The 13 nm satellite AuNPs were modified with a thiolated catalytic DNA hairpin (H) and a Raman reporter 4-ATP. The 50 nm core AuNPs were functionalized with another thiolated catalytic DNA hairpin (SS) and a swing arm single stranded DNA (SA) that was partially hybridized with an aptamer (Ap) which can specifically recognize the EpCAM. These two types of AuNPs functionalized with different components are named as Au_{13}–H and Au_{50}–SS–SA–Ap, respectively. When Au_{13}–H and Au_{50}–SS–SA–Ap were present together with the EpCAM-positive cells, the specific binding between the aptamer and EpCAM on the cell membrane surface can free the SA strand on the 50 nm AuNP surface. Meanwhile, SA possesses a toehold region that can hybridize with the adjacent SS strand to form an intermediate SA–SS complex. With the help of the H strand that was anchored on the 13 nm AuNP, these SA–SS intermediates can form a more stable SS–H duplex *via* toehold-mediated strand displacement and release the SA strand for the next cycle of catalyzation on the 50 nm AuNP surface. In this way, a single target molecule (EpCAM) on the live cell surface was able to trigger the autonomous assembly of the two hairpins and assemble multiple 13 nm AuNPs on the surface of 50 nm AuNPs, thus changing the state of the whole colloidal structures from spatially separated particles to a core–satellite assembly. Meanwhile, because of the interparticle plasmonic coupled hot spots generated in the core–satellite nanostructures, enhanced Raman scattering of 4-ATP molecules can be used to accurately capture the dynamic structural change of the nanostructures in response to the cell surface marker.

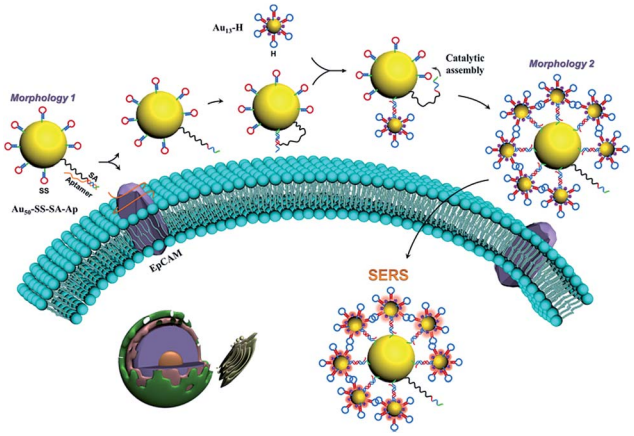

Fig. 1 Schematic representation of the dynamic assembly of the core–satellite nanostructure from Morphology 1 to Morphology 2 triggered by EpCAM receptors on the cell membrane surface.

We separately verified the functional components in this system step by step. First, to ensure that the partially hybridized SA–Ap duplex strand can be responsive to EpCAM protein,[32] the FRET-based SA–Ap duplex with a fluorophore (SA-FAM) and quencher (BHQ_1–Ap) pair was employed to monitor the competitive binding process between EpCAM–Ap and SA–Ap. The sequence length of SA_0 (the functional domain of SA that can catalyze the subsequent reaction) plays an important role in ensuring the efficient separation of the SA and Ap duplex upon EpCAM as well as the low background "leaky" reaction without the presence of the EpCAM. In our design, 20 nucleotides (nts) were chosen as the length of the SA–Ap complementary duplex with a good signal to background ratio (Fig. S2†).

Once confirmed that our system can respond to the EpCAM and expose the active catalytic DNA domain (SA_0) on SA effectively, we continued to optimize the subsequent DNA catalytic hairpin reactions to improve the nanoparticle assembly

efficiency. As shown in Fig. 2A, SA_0 contains toehold domain 1* that can hybridize with the exposed domain 1 on SS to initiate the strand displacement and domain 2* that can trigger the branch migration to the fully open hairpin structure of SS. In addition, loop domain 3 on the SS strand should also play important roles in the catalytic hairpin reactions. Therefore, we separately investigated the sequence length of domains 1, 2 and 3 on SS to achieve the highest catalytic efficiency as well as the lowest background signal of SS and H without SA. To ensure the structural stability of the SS strand, we chose 14 nts as the length of stem domain 2, and then studied 4 cases of different lengths of domain 1 and domain 3, respectively. As shown in Fig. 2B and C, we used the ratio of products (group with SA + SS + H) to "leaky" reaction byproducts (SS + H) to evaluate the hairpin catalytic reaction efficiency. It can be seen that case 1 (domain 1 = 6 nt, domain 3 = 15 nt) achieved the highest signal to noise ratio (Fig. 2D). Therefore, SS_1 and H_1 were chosen as the optimal sequences for the subsequent nanoparticle assembly.

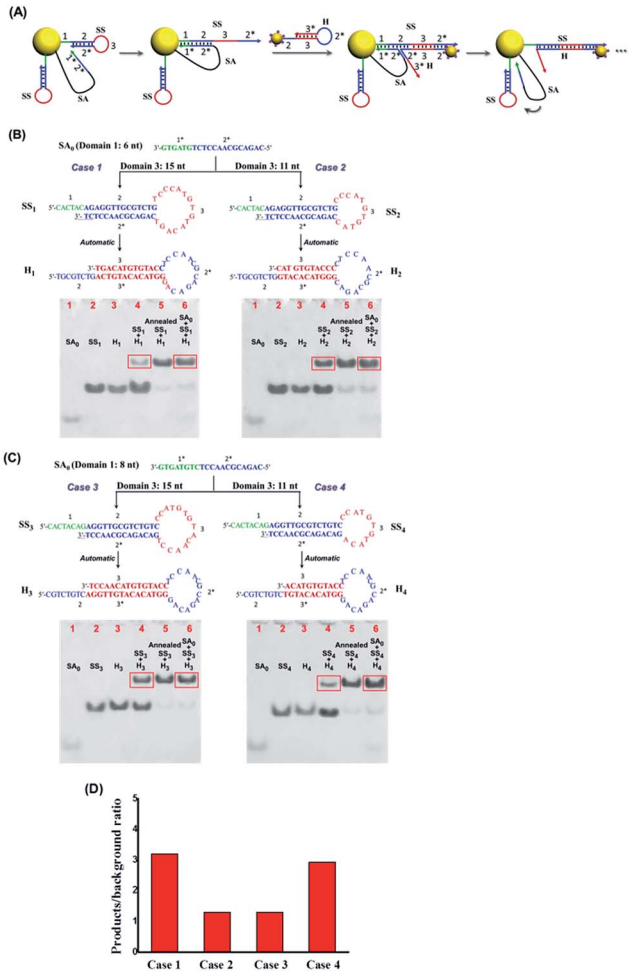

Fig. 2 (A) Scheme of the catalytic hairpin assembly reaction triggered by toehold-mediated strand displacement. (B and C) Optimization and PAGE characterization of the sequences designed for the dynamic colloidal nanoparticle system. (D) Comparison of the ratio of products (group with SA + SS + H) to "leaky" reaction byproducts (SS + H). Here, we use NUPACK (http://www.nupack.org) to predict the secondary structures of the DNA strands.

We subsequently performed a feasibility test to determine whether the DNA hairpin catalytic reaction can facilitate the assembly of Au nanoparticles to form the core–satellite structure in solution. The morphological changes of the system can be monitored by optical property measurements that are sensitive to the distance between neighboring particles, such as SERS and surface plasmon resonance (SPR). First, we used the SS_1, H_1 and an unblocked SA as the optimal sequence combination in terms of assembly efficiency to study the dynamic assembly of the core–satellite nanostructure by SPR (Fig. 3A). Meanwhile, a 20 bp complementary SA–Ap duplex was used as a control group to verify the assembly background signal of the system without the presence of the EpCAM. Notably, we used a molar ratio of 10 : 1 of SS_1 and SA to modify the 50 nm AuNP surface. Considering the catalytic efficiency of a similar hairpin system reported by Chen, one SA molecule should be able to catalyze 20–50 hairpins to form a stable duplex.[37] However, the spatial steric effect generated by 13 nm AuNPs assembled on the surface of 50 nm AuNPs is another factor to consider, as too many 13 nm AuNPs would hinder the further assembly. Therefore, in this scenario, we chose a 10 : 1 ratio for SS_1 and SA as the optimum condition to functionalize the 50 nm AuNPs. Following 12 h incubation of Au_{13}–H_1 with Au_{50}–SS_1–SA–Ap and Au_{50}–SS_1–SA, respectively, the products were examined by UV-vis absorption spectra and dynamic light scattering (DLS) (Fig. 3B and C). Compared to Au_{13}–H_1 only (curve a in Fig. 3B), Au_{50}–SS_1–SA only (curve b in Fig. 3B) and mixtures of Au_{50}–SS_1–SA–Ap and Au_{13}–H_1 (curve c in Fig. 3B), the absorption peak of Au_{50}–SS_1–SA + Au_{13}–H_1 mixtures showed a significant red shift from about 530 nm to 552 nm (curve (d) in Fig. 3B), indicating strong surface plasmon resonance happening in the assembly. Combined with the obvious increase of hydrodynamic diameters from 66.44 ± 2.27 nm (curve b in Fig. 3C) with Au_{50}–SS_1–SA only to 102.40 ± 8.19 nm (curve d in Fig. 3C), it is believed that the core–satellite assemblies were formed. We further used transmission electron microscopy (TEM) to visualize the structures. When mixing Au_{50}–SS_1–SA–Ap with Au_{13}–H_1, it can be seen that 50 nm AuNPs were surrounded by only six 13 nm AuNPs in close proximity on average, which is believed to be induced by the "leaky" reaction of the hairpin assembly (Fig. 3D and F). However, the number of "satellites" surrounding the "core" increased to 14 on average when mixing Au_{50}–SS_1–SA with Au_{13}–H_1 (Fig. 3E and F). These observations verified that the dynamic assembly of Au nanoparticles can be formed and controlled by the SA strand.

Next, we used SERS to further monitor the dynamic assembly process of the system in solution. 4-ATP was adsorbed on the 13 nm AuNPs as a Raman reporter. As shown in Fig. 3G, Au_{50}–SS_1–SA and Au_{50}–SS_1–SA–Ap both displayed no Raman signal due to the absence of Raman reporters. Au_{13}–H_1 can generate a weak SERS signal because of the insufficient electromagnetic coupling on its surface. When mixing Au_{50}–SS_1–SA with Au_{13}–H_1 probes, strong characteristic peaks of 4-ATP at 1078 cm^{-1} and 1585 cm^{-1} were observed, indicating the formation of electromagnetic hot spots with proximity of Au nanoparticles. Meanwhile, as for the mixture of Au_{50}–SS_1–SA–Ap and Au_{13}–H_1, the SERS peak intensities were much weaker and just similar to

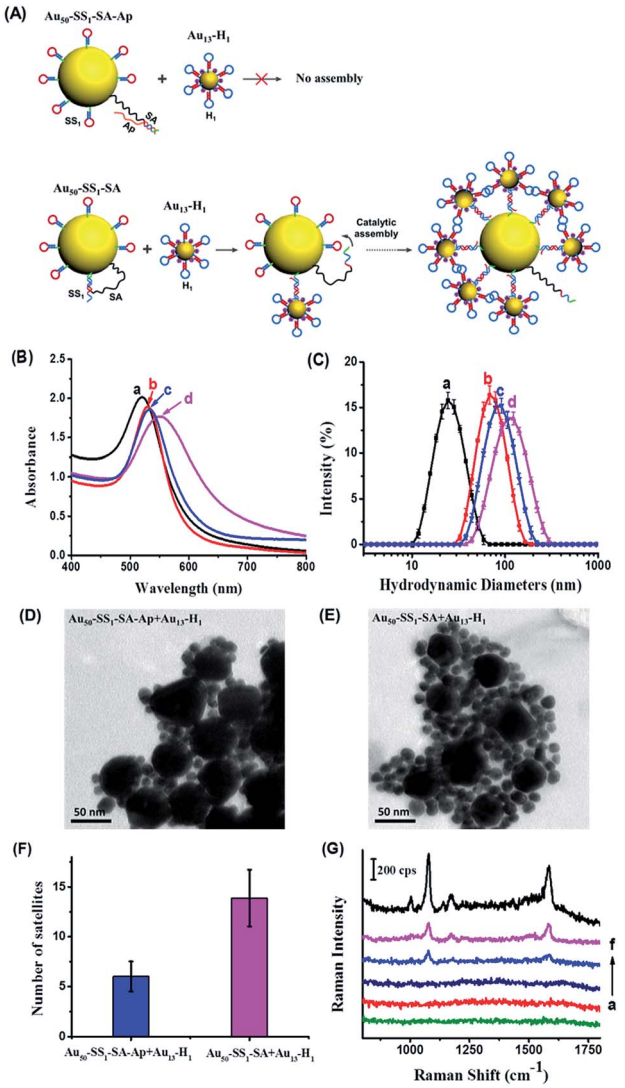

Fig. 3 (A) Scheme of blocked and unblocked SA-triggered assembly of the core–satellite nanostructures. (B) UV-vis absorption spectra and (C) DLS intensity of (a) Au_{13}–H_1 only, (b) Au_{50}–SS_1–SA only, (c) mixtures of Au_{50}–SS_1–SA–Ap and Au_{13}–H_1, (d) mixtures of Au_{50}–SS_1–SA and Au_{13}–H_1. (D) TEM image of mixtures of Au_{50}–SS_1–SA–Ap and Au_{13}–H_1. (E) TEM image of mixtures of Au_{50}–SS_1–SA and Au_{13}–H_1. (F) Average numbers of 13 nm "satellite" nanoparticles of groups Au_{50}–SS_1–SA–Ap + Au_{13}–H_1 and Au_{50}–SS_1–SA + Au_{13}–H_1. The numbers were summarized by counting 30 "core" nanoparticles in each group in the TEM images. (G) SERS signals of (a) the mixture of SS_1, H_1, SA and Ap without AuNPs; (b) Au_{50}–SS_1–SA only; (c) Au_{50}–SS_1–SA–Ap only; (d) Au_{13}–H_1 only; (e) mixture of Au_{50}–SS_1–SA–Ap and Au_{13}–H_1; (f) mixture of Au_{50}–SS_1–SA and Au_{13}–H_1.

those of Au_{13}–H_1 only. The finite difference time domain (FDTD) simulations were employed to theoretically calculate the enhanced electromagnetic field distribution of the core–satellite nanostructure. The electromagnetic field intensity in the gap between assembled 13 nm and 50 nm AuNPs was found to be much stronger than that on the 13 nm AuNP surface (Fig. S3†). Therefore, combining both the experimental and theoretical findings, the newly generated interparticle plasmonic coupled hot spots in the core–satellite nanostructures can provide strong SERS signals. It also paved ways for using SERS to reveal the dynamic assembly activated by aptamer–receptor interactions on live cell membranes.

Last, we determined whether we could activate the dynamic assembly of nanoparticles by aptamer–receptor interactions on live cell membranes. Specifically, we chose the EpCAM-positive cell line MCF-7, a cell line originating from human breast adenocarcinoma cells, as the target cell to test the assembly of the nanoparticle system. The EpCAM-negative cell line HEK-293T, derived from human embryonic kidney cells, was used as the control cell line. Prior to application of the nanoparticles to living cells, the cytotoxicity of Au_{13}–H_1 and Au_{50}–SS_1–SA–Ap was checked to investigate the influence of nanoparticles on the cell status after a relatively long incubation. The viabilities of the two cell lines were found to be almost unaffected by the concentrations and incubation time used for the cell experiment (Fig. S4†).

MCF-7 cells were incubated with Au_{50}–SS_1–SA–Ap and Au_{13}–H_1 for 12 h to make sure that the Au_{50}–SS_1–SA–Ap can sufficiently interact with EpCAM receptors on the cell membrane surface, assemble with Au_{13}–H_1 on the membranes and then internalize into the cells. Fig. 4 shows that the Raman signals of MCF-7 cells with different nanoparticle groups are acquired in the 1078 cm^{-1} channel. The typical Raman scattering peak of 4-ATP at 1078 cm^{-1} enhanced more significantly than that at 1585 cm^{-1}, so the peak at 1078 cm^{-1} was used to map the cells. With addition of Au_{50}–SS_1–SA–Ap only, there was no signal due to the lack of Raman reporters. When MCF-7 cells were treated with Au_{13}–H_1 probes only, they exhibited a weak Raman signal which corresponded to the relatively insufficient enhancement of Raman scattering on the 13 nm AuNP surface. Notably, MCF-7 cells treated with both Au_{50}–SS_1–SA–Ap and Au_{13}–H_1 together generated a significantly enhanced Raman signal, indicating that core–satellite nanoassemblies were formed in the cellular environment. In addition, with the presence of Au_{50}–SS_1–SA and Au_{13}–H_1 probes, the Raman scattering of MCF-7 cells was also enhanced significantly, confirming that the unblocked SA is the key to initiate the strand displacement and change the dynamic system into a core–satellite structure in living cells (Fig. S5†).

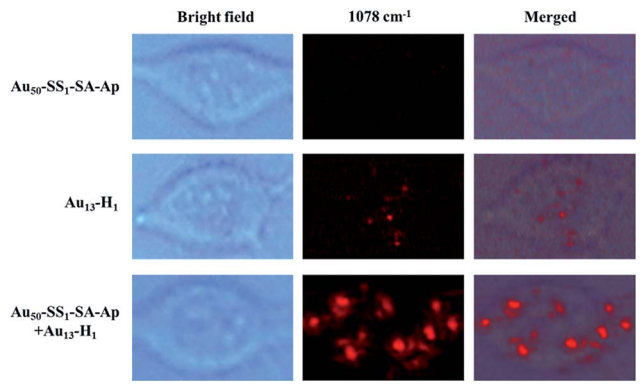

Fig. 4 Bright field and Raman images of MCF-7 cells which were treated with Au_{50}–SS_1–SA–Ap (0.02 nM), Au_{13}–H_1 (0.5 nM) only and the mixture of Au_{50}–SS_1–SA–Ap (0.02 nM) and Au_{13}–H_1 (0.5 nM).

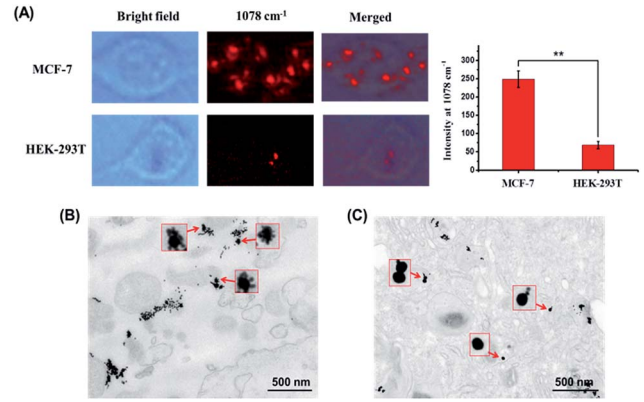

Fig. 5 (A) Bright field and Raman images of MCF-7 cells and HEK-293T cells treated with both Au_{50}–SS_1–SA–Ap (0.02 nM) and Au_{13}–H_1 (0.5 nM) (** stands for p values < 0.01, $n = 10$). TEM images of 100 nm thick cell sections were derived from (B) MCF-7 and (C) HEK-293T cells incubated with both Au_{50}–SS_1–SA–Ap (0.02 nM) and Au_{13}–H_1 (0.5 nM). The insets show the enlarged pictures of the particles.

Then we studied the nanoparticle assembly in EpCAM-negative cell line HEK-293T to determine whether the enhanced Raman signals were derived from the presence of the EpCAM receptor on the cell membrane surface. After 12 h incubation, a much weaker Raman signal compared to that of MCF-7 cells in the 1078 cm^{-1} channel was seen (Fig. 5A). We also summarized the mean Raman signal intensities of 10 different MCF-7 and HEK-293T cells. It can be seen that they are significantly different with a p value of 0.002. In addition, TEM images of 100 nm thick cell sections were compared and are shown in Fig. 5B and C. Core–satellite assembly structures were found in the MCF-7 cells, whereas mainly separated particles were seen in HEK-293T cells. These data verified that the cell-surface EpCAM can trigger the dynamic assembly of nanoparticles from separated particles to a core–satellite structure and also confirmed the credibility of our assembly strategy in complex biological environments.

Conclusions

Design of dynamic systems with such capabilities as conformation or function change in response to biological signals in biological environments is an important step toward intelligent diagnosis and disease treatment. In this study, we have engineered a dynamic system based on aptamer–receptor interactions and DNA displacement reactions to autonomously assemble core–satellite nanostructures in the cellular environment, owing to the combination of the high specificity of the aptamer and the stable performance of DNA catalytic reactions. The structural changes of the dynamic system have provided electromagnetic hot spots for SERS imaging to precisely characterize the systems in complex biological milieus.

Compared with dynamic systems based totally on DNA base-pairing, the introduction of an aptamer provides a direct molecular bridge linking DNA with proteins on cell membranes, enabling precise sensing of the cellular environment and smart control of the dynamic assembly process *in situ*. Moreover, as a variety of aptamers are either available or can be obtained through SELEX to bind a broad range of targets with tunable binding ability, the proposed dynamic system also provided a versatile tool responsive to other biological targets in cellular context by simply changing the aptamers. Given the design modularity with DNA displacement reactions and target specificity with aptamers, the prototype aptamer–receptor interaction triggered dynamic system demonstrated here has the potential to enhance DNA nanotechnology with new insights and will broaden the utility of dynamic nanomaterials for applications in biology, biotechnology and biomedicine, such as development of future smart nanomaterials that combine autonomous delivery, transformation and activation functions in the blood stream to diagnose or treat targeted sites.

Conflicts of interest

There are no conflicts to declare.

Acknowledgements

This project was financially supported by the National Sciences Foundation of China (Grant No. 21675134). Da Han acknowledges start-up funding support from the Institute of Molecular Medicine of Shanghai Jiao Tong University and the 1000 Youth Talents Program, granted by the Chinese Central Government.

Notes and references

1 L. Lin, Y. Xie, S. Wang, W. Wu, S. Niu, X. Wen and Z. L. Wang, *ACS Nano*, 2013, 7, 8266–8274.
2 M. Yasui, M. Hiroshima, J. Kozuka, Y. Sako and M. Ueda, *Nat. Commun.*, 2018, **9**, 3061.
3 G. Yu, B. C. Yung, Z. Zhou, Z. Mao and X. Chen, *ACS Nano*, 2018, **12**, 7–12.
4 J. Kim, D. Jang, H. Park, S. Jung, D. H. Kim and W. J. Kim, *Adv. Mater.*, 2018, **30**, 1707351.
5 S. Ohta, D. Glancy and W. C. W. Chan, *Science*, 2016, **351**, 841–845.
6 C. Wong, T. Stylianopoulos, J. Cui, J. Martin, V. P. Chauhan, W. Jiang, Z. Popović, R. K. Jain, M. G. Bawendi and D. Fukumura, *Proc. Natl. Acad. Sci. U. S. A.*, 2011, **108**, 2426–2431.
7 H. Park, J. Kim, S. Jung and W. J. Kim, *Adv. Funct. Mater.*, 2018, **28**, 1705416.
8 N. C. Seeman, *Trends Biotechnol.*, 1999, **17**, 437–443.
9 F. Zhang, J. Nangreave, Y. Liu and H. Yan, *J. Am. Chem. Soc.*, 2014, **136**, 11198–11211.
10 Y.-J. Chen, B. Groves, R. A. Muscat and G. Seelig, *Nat. Nanotechnol.*, 2015, **10**, 748–760.
11 A. J. Thubagere, W. Li, R. F. Johnson, Z. Chen, S. Doroudi, Y. L. Lee, G. Izatt, S. Wittman, N. Srinivas, D. Woods, E. Winfree and L. Qian, *Science*, 2017, **357**, eaan6558.
12 R. A. Muscat, J. Bath and A. J. Turberfield, *Nano Lett.*, 2011, **11**, 982–987.

13 M. Hagiya, A. Konagaya, S. Kobayashi, H. Saito and S. Murata, *Acc. Chem. Res.*, 2014, **47**, 1681–1690.
14 T.-G. Cha, J. Pan, H. Chen, J. Salgado, X. Li, C. Mao and J. H. Choi, *Nat. Nanotechnol.*, 2014, **9**, 39–43.
15 H. Peng, X. F. Li, H. Zhang and X. C. Le, *Nat. Commun.*, 2017, **8**, 14378–14390.
16 P. Q. Ma, C. P. Liang, H. H. Zhang, B. C. Yin and B. C. Ye, *Chem. Sci.*, 2018, **9**, 3299–3304.
17 Y. Tian, Y. He, Y. Chen, P. Yin and C. D. Mao, *Angew. Chem., Int. Ed.*, 2005, **44**, 4355–4358.
18 M. You, Y. Chen, X. Zhang, H. Liu, R. Wang, K. Wang, K. R. Williams and W. Tan, *Angew. Chem., Int. Ed.*, 2012, **51**, 2457–2460.
19 X. Qu, D. Zhu, G. Yao, S. Su, J. Chao, H. Liu, X. Zuo, L. Wang, J. Shi, L. Wang, W. Huang, H. Pei and C. Fan, *Angew. Chem., Int. Ed.*, 2017, **56**, 1855–1858.
20 Y. Yang, M. A. Goetzfried, K. Hidaka, M. You, W. Tan, H. Sugiyama and M. Endo, *Nano Lett.*, 2015, **15**, 6672–6676.
21 Q. H. Liu, L. M. Wang, A. G. Frutos, A. E. Condon, R. M. Corn and L. M. Smith, *Nature*, 2000, **403**, 175–179.
22 L. Qian and E. Winfree, *Science*, 2011, **332**, 1196–1201.
23 L. Qian, E. Winfree and J. Bruck, *Nature*, 2011, **475**, 368.
24 F. Chen, M. Bai, K. Cao, Y. Zhao, X. Cao, J. Wei, N. Wu, J. Li, L. Wang, C. Fan and Y. Zhao, *ACS Nano*, 2017, **11**, 11908–11914.
25 J. Liu, M. Cui, H. Zhou and W. Yang, *ACS Sens.*, 2017, **2**, 1847–1853.
26 J.-J. Li, W.-N. Li, W.-F. Du, M.-M. Lv, Z.-K. Wu and J.-H. Jiang, *Chem. Commun.*, 2018, **54**, 10626–10629.
27 X. Fang and W. Tan, *Acc. Chem. Res.*, 2010, **43**, 48–57.
28 C. Liu, J. Zhao, F. Tian, L. Cai, W. Zhang, Q. Feng, J. Chang, F. Wan, Y. Yang, B. Dai, Y. Cong, B. Ding, J. Sun and W. Tan, *Nat. Biomed. Eng.*, 2019, **3**, 183–193.
29 D. Han, Z. Zhu, C. Wu, L. Peng, L. Zhou, B. Gulbakan, G. Zhu, K. R. Williams and W. Tan, *J. Am. Chem. Soc.*, 2012, **134**, 20797–20804.
30 H.-M. Meng, H. Liu, H. Kuai, R. Peng, L. Mo and X.-B. Zhang, *Chem. Soc. Rev.*, 2016, **45**, 2583–2602.
31 M. Munz, P. A. Baeuerle and O. Gires, *Cancer Res.*, 2009, **69**, 5627–5629.
32 Y. Song, Z. Zhu, Y. An, W. Zhang, H. Zhang, D. Liu, C. Yu, W. Duan and C. J. Yang, *Anal. Chem.*, 2013, **85**, 4141–4149.
33 J. Song, J. Zhou and H. Duan, *J. Am. Chem. Soc.*, 2012, **134**, 13458–13469.
34 Y. Chen, L. Ding, W. Song, M. Yang and H. Ju, *Chem. Sci.*, 2016, **7**, 569–574.
35 W. Zhou, Q. Li, H. Liu, J. Yang and D. Liu, *ACS Nano*, 2017, **11**, 3532–3541.
36 C. Zong, M. Xu, L.-J. Xu, T. Wei, X. Ma, X.-S. Zheng, R. Hu and B. Ren, *Chem. Rev.*, 2018, **118**, 4946–4980.
37 B. Li, A. D. Ellington and X. Chen, *Nucleic Acids Res.*, 2011, **39**, e110.